Analysis of mixing in three-dimensional time-periodic cavity flows

By P. D. ANDERSON, O. S. GALAKTIONOV†
G. W. M. PETERS, F. N. van de VOSSE
and H. E. H. MEIJER

Materials Technology, Dutch Polymer Institute, Eindhoven University of Technology,
P.O. Box 513, 5600 MB Eindhoven, The Netherlands

A method to locate periodic structures in general three-dimensional Stokes flows with time-periodic boundary conditions is presented and applied to mixing cavity flows. Numerically obtained velocity fields and particle tracking schemes are used to provide displacement and stretching fields. From these the location and identification of periodic points can be derived. The presence or absence of these periodic points allows a judgement on the quality of the mixing process. The technique is general and efficient, and applicable to mixing flows for which no analytical velocity field is available (the case for all three-dimensional flows considered in this paper). Results are presented for three different mixing protocols in a three-dimensional time-periodic cavity flow, serving as an accessible test case for the methods developed. A major result is that *periodic lines* are obtained for these three-dimensional flows. These lines can be complex in geometry and their nature can change along a line from hyperbolic to elliptic. They can serve as practical criteria in the optimization of three-dimensional mixing processes.

1. Introduction

Several experimental and computational studies have demonstrated the effectiveness of chaotic mixing in low Reynolds number flows. Much of these studies serve to clarify the fundamentals of mixing processes. A thorough review of the key concepts in chaotic mixing can be found in Ottino (1990). Numerous studies on two-dimensional flows have been summarised by Chien, Rising & Ottino (1986), Ottino (1989) and Jana, Metcalfe & Ottino (1994). Recently, some papers have appeared that report on mixing experiments and simulations involving three-dimensional flows (see Kusch & Ottino 1992; Miles, Nagarajan & Zumbrunnen 1995; Southerland, Frederiksen & Dahm 1995; Cartwright Feingold & Pirol 1996; Avalosse & Crochet 1997; Hobbs & Muzio 1997). In this study a method is introduced to analyse mixing in three-dimensional flows and results are presented for three-dimensional cavity flows, which are considered to act as prototypes for studying mixing processes.

It is well known that in steady two-dimensional cavity Stokes flows, the velocity field is integrable and the flow is non-chaotic (Aref 1984). A tracer in the flow follows closed streamlines, and, as a consequence, mixing is poor, since the tracer only travels through a limited part of the flow domain and the stretching in the steady flow will only be linear. If, however, the flow is made time-periodic, it is very likely that the

† Permanent address: Institute of Hydromechanics, Kiev, Ukraine.

system will possess chaotic trajectories. In this case a tracer is no longer trapped by closed streamlines and is advected to a larger portion of the flow domain. The stretching may become exponential, resulting in efficient mixing, e.g. Ottino (1989).

The main characteristics of chaotic mixing are determined by the location and nature of the periodic points. By definition, periodic points are points which return to their original position after one or more periods of flow. They are classified according to the nature of the deformation in their neighbourhood. Elliptic (stable) periodic points are at the centre of non-mixing regions, called islands, while hyperbolic (unstable) periodic points are centres of stretching and folding in the flow. Around hyperbolic points the fluid is compressed in one eigendirection and stretched in the other eigendirection. In this paper, only first-order periodic points are investigated. While considerable theoretical guidance exits for two-dimensional closed time-periodic mixing flows, there is a lack of similar tools and results for complex three-dimensional flows.

The primary objective of this study, is to extend methods and concepts available for two-dimensional flows to analyse mixing in general three-dimensional cavity flows. Because of computational restrictions associated with large three-dimensional problems, our analysis for now is limited to the first period of a time-periodic flow. The algorithm presented in this paper can however also be used to determine higher-order periodic points, and it is not limited by special requirements with respect to the geometry of the mixing flow or by the rheology of the fluid. It consists of the following steps: first, an accurate representation of the velocity field is computed; next, adaptive particle tracking is used to determine the deformation of well-defined material volumes, and displacement data in the flow are used to locate points returning after one period; finally, stretching data are used to determine the nature of the periodic points. The term *periodic structures* is used to represent the set of periodic points.

A first approach for determining periodic points in three-dimensional flows was to extend an existing method for two-dimensional time-periodic lid-driven cavity flows (Meleshko & Peters 1996) to three-dimensional cavity flows. This technique, however, exploits some symmetry in the velocity field and therefore has limited application. If the technique is applied to the three-dimensional cavity with closed top and bottom, where the flow is induced by the time-periodic motion of the front and back walls, some non-trivial results are obtained. The periodic points found form periodic lines in the flow domain. It is also observed that the nature of the periodic points on these lines can change if one travels along a periodic line. For the three-dimensional flows considered in this paper, the periodic lines are closed or start and end on the boundary of the flow domain.

For more general three-dimensional flows, considerations like symmetry do not apply and, therefore, in this paper an additional algorithm is introduced that locates regions with minimum displacement after one period of mixing in order to identify periodic structures. To validate the technique, it is shown that its application to quasi-two-dimensional two-step time-periodic three-dimensional flows yields the same periodic structures as found earlier, using the method exploiting symmetry. A four-step mixing protocol to obtain a fully three-dimensional flow is introduced, and elliptic and hyperbolic periodic lines are determined. The differences in mixing performance for blobs placed at different positions, around different type of periodic points in the three-dimensional cavity, are already obvious by as few as four periods of flow.
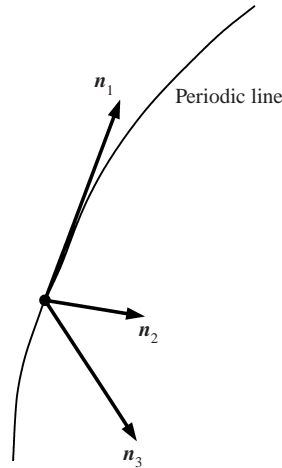
FIGURE 1. Search algorithm for a periodic line. The eigenvector n_1 corresponding the eigenvalue 1 is tangential to the periodic line.

2. Periodic structures in three-dimensional mixing flows

In this section the algorithms to locate and classify periodic points in three-dimensional mixing flows are presented. It is observed that for certain three-dimensional flows these points can form open or closed lines, and since the structure of the lines is not clear in advance, we denote the collection of periodic points as a periodic structure. Two possibilities are distinguished: flows where a symmetry condition can be used to reveal the periodic points and more general flows where such a symmetry condition is absent or too complicated to be of use for the analysis of periodic points. Results obtained with the first type of flow can be used to check the more general method.

In general any flow can be represented by

$$x = \Phi_t(X), \qquad X = \Phi_{t=0}(X), \qquad (2.1)$$

mapping particle X to x after a time t, e.g. Ottino (1989), where X refers to the initial position at $t = 0$.

Using this definition, a periodic point P of order n is defined as

$$\Phi_{n\,T}(P) = P, \qquad (2.2)$$
$$\Phi_{m\,T}(P) \neq P \text{ for } m < n. \qquad (2.3)$$

T is the duration of one period of motion.

2.1. *Determination of periodic structures using symmetry of the flow*

For cavity flow with time-periodic motion of the front and back walls only in the x-direction (defined as protocol $\mathscr{A}$ in §4.2 and shown in figure 2), periodic points can be found using a technique similar to that elaborated by Meleshko & Peters (1996). This technique, originally designed for two-dimensional cavity flow, exploits symmetry in the velocity field (streamlines are symmetrical with respect to the plane $x = 0$ (see also Bajer 1995)) and is, with minor adaptations, also applicable to three-dimensional cavity flow. The essential knowledge about periodic points is that they cross the plane of symmetry, say $x = 0$, at the times $t = T/4$ and $t = 3T/4$ (where T is again the time of one period). So, the surface that coincides with the plane $x = 0$ at the

instant $t = T/4$ is tracked up to the time $t = 3T/4$. The intersection of this deformed surface with the plane $x = 0$ gives a portrait of the periodic structures, namely their positions after $3/4$ periods of the motion. In general the intersection of the two surfaces can consist of surfaces, lines and points. For the results presented here, the intersections (and thus the periodic structures) consist of lines which are closed or end at the boundary (since the deformed surface and the plane $x = 0$ have a common boundary). The true position of the periodic lines is found by tracking the points to the time $t = T$. The location of the points was also verified by tracking them for one complete period of the flow. An example of this technique is presented in §4.3.

2.2. *Determination of periodic structures in general periodic flows*

For more general three-dimensional mixing flows, considerations like symmetry in the velocity field can be of no use. This implies that another technique for finding periodic structures is needed. The technique developed here is based on an analysis of displacement and stretching over one period. The displacement function is defined as

$$d(X) = \|X - \Phi_T(X)\|_2, \tag{2.4}$$

where $\| \cdots \|_2$ is the Euclidean norm.

Using the definition of the displacement gradient $F_X = (\nabla_X \Phi_T(X))^T$, a useful definition of the stretching coefficient can be formed:

$$s(X) = \max_{\lambda \in \sigma(F_X)} |\lambda|, \tag{2.5}$$

where $\sigma(F_X)$ is the eigenvalue spectrum of F_X.

The technique used to locate periodic points is essentially based on finding roots of $d(X) = 0$. If a root is found, say point x_0, then the eigenvalues λ_1, λ_2 and λ_3 of the displacement gradient matrix F_X are investigated. Notice that for incompressible fluids $\det(F_X) = 1$ or, equivalently, $\lambda_1 \lambda_2 \lambda_3 = 1$. If (and only if) the periodic point x_0 belongs to a periodic line, which is mapped to itself, one of the eigenvalues (say, λ_1) is necessarily equal to 1. If a periodic point is found with an eigenvalue 1 then the eigenvectors are used to search for other periodic points. It is used that the corresponding eigenvector n_1 is tangential to the periodic line (see figure 1). This is clear since

$$\alpha n_1 = F_{x_0} \cdot \alpha n_1 = \alpha \lambda_1 n_1 \qquad (\alpha \to 0). \tag{2.6}$$

For the other two eigenvalues there are two possibilities.

(*a*) First, both of them can be complex and then they are complex conjugate: $\lambda_2 = \lambda_3^*$ and $\lambda_2 \lambda_3 = 1$. Their absolute values are in this case both equal to 1 and the type of the periodic point on the line is elliptic (locally the material rotates around the periodic point).

(*b*) The other possibility is that both eigenvalues λ_2 and λ_3 are real. In the limiting case (parabolic point) the absolute value of both of them can be equal to 1, otherwise the absolute value of one of them is larger than 1, and as previously $\lambda_2 \lambda_3 = 1$. This corresponds to an unstable (hyperbolic) point on the line (locally the material is stretched).

Note that the term 'elliptic' can be somewhat misleading for the three-dimensional case: in the vicinity of a stable periodic point, a combination of rotation and, perpendicular to that, shear can occur. In the two-dimensional case the combination of shear and rotation around a stable periodic point is not possible.
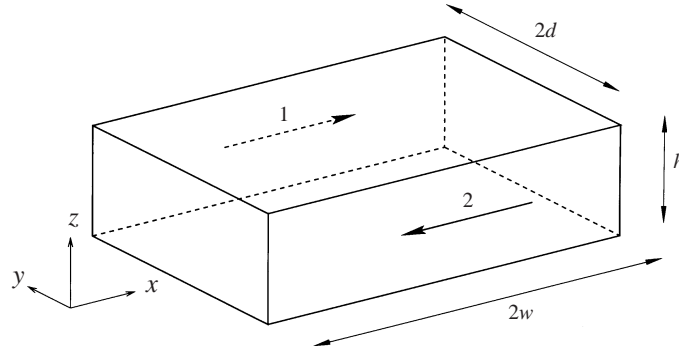
FIGURE 2. Geometry and definition of the cavity flow; arrow 1 depicts the movement of the front wall, arrow 2 that of the back wall, all other walls are stationary.

3. Computational issues

Figure 2 shows the geometry investigated in this paper: a three-dimensional rectangular cavity $-w < x < w$, $-d < y < d$, $0 < z < h$. The front and back walls can be moved tangentially with velocities $\boldsymbol{u}_F$ and $\boldsymbol{u}_B$ respectively, the other walls are stationary. The boundary conditions for the velocities $\boldsymbol{g}$ are

$$
\boldsymbol{g} = \begin{cases} \boldsymbol{u}_F = U_F(t)\, \boldsymbol{e}_x + W_F(t)\, \boldsymbol{e}_z & \text{at } y = -d, \\ \boldsymbol{u}_B = U_B(t)\, \boldsymbol{e}_x + W_B(t)\, \boldsymbol{e}_z & \text{at } y = d, \\ \boldsymbol{0} & \text{other walls .} \end{cases} \tag{3.1}
$$

The time-periodic wall motions are discontinuous and co-rotational in time, e.g. the front and back walls move in opposite directions. Since highly viscous fluids are assumed, the Reynolds numbers are small, and a Stokes approximation is used. The velocity field $\boldsymbol{u}$ of the flow in the domain Ω is then described by the steady Stokes equations,

$$
\begin{cases} v\nabla^2 \boldsymbol{u} - \nabla p = 0 & \text{in } \Omega, \\ \nabla \cdot \boldsymbol{u} = 0 & \text{in } \overline{\Omega}, \\ \boldsymbol{u} = \boldsymbol{g} & \text{on } \partial\Omega, \end{cases} \tag{3.2}
$$

where v is the kinematic viscosity of the Newtonian fluid, p is the pressure and $\overline{\Omega}$ is the closure of Ω.

The solution of the stationary Stokes equations (3.2) is computed as an asymptotic case of the unsteady equations. A continuous projection method is used to decouple the velocity and pressure components (see Gresho 1990; Timmermans, Minev & Vosse 1996). The original problem is reformulated into four simpler problems: the solution of a Helmholtz problem for each of the velocity components and a Poisson equation for the pressure. The Helmholtz and Poisson problems are discretised in space using the spectral element method, introduced by Patera (1984) and further developed by Maday & Patera (1989). For a more detailed description of this numerical scheme see Timmermans *et al.* (1996) and Minev *et al.* (1995).

In numerical collocation schemes the velocity is only known at a limited number of grid points. Tracking material points in a flow requires knowledge of the velocity of the fluid at any arbitrary point in the flow domain. Therefore, interpolation

of the velocity field to a set of arbitrary points is necessary. The accuracy of the interpolation is always limited to the accuracy of the discretised data. To ensure that the interpolation error is of the same order as the approximation error (of the discretised data) a consistent interpolation scheme is necessary: a scheme that uses the same polynomial basis functions as are used within the numerical discretisation. Souvaliotis, Jana & Ottino (1995) studied the influence of small disturbances in the velocity field which give rise to completely different advection patterns for chaotic mixing flows.

The strategies to locate periodic points described in §§ 2.1 and 2.2 require an accurate tracking of material volumes. The tracking of these volumes involves the numerical integration of the dynamical system

$$\dot{\boldsymbol{x}} = \boldsymbol{u}(x, y, z, t), \tag{3.3}$$

which is computationally expensive if the velocity field is not analytically available. A fourth-order adaptive Runge–Kutta scheme (see Press *et al.* 1992) is used to solve equation (3.3) and to make sure that time integration errors can be neglected compared to the spatial discretisation errors. To follow material volumes and surfaces in the flow, some conventional methods (Carey & Chen 1995; Ottino, Souvaliotis & Metcalfe 1995) uniformly distribute a large number of points in the volume and track them individually. For three-dimensional applications in particular this strategy requires exceptional computational resources to obtain satisfactory precision. A possible way out consists in tracking just the boundary of the selected volume. Nevertheless, as the material volume is stretched and folded many times in case of periodic laminar mixing, it is important to choose an appropriate strategy for the representation of the volume. Although various techniques of adding new material points are available (based, for example, on local smoothing of the curve using splines), the addition of auxiliary material points onto the initial configuration is preferred, since this configuration is supposed to be defined exactly. Analysis of distance and curvature between adjacent material points is performed and when necessary additional points are inserted. With this approach an accumulation of errors is avoided, and at all times an accurate representation of the material volume is available.

The general strategy to find first-order periodic structures in three-dimensional flows requires the computation of the displacement function $d(\boldsymbol{X})$ within the flow domain. To locate the roots of $d(\boldsymbol{X}) = 0$ the following strategy is used:

(*a*) Analysis of marker displacement on a coarse three-dimensional grid over one period, to find an initial guess for the local minimum of displacement. See figure 3(*a*).

(*b*) Accurate determination of the position of local minima of displacement, using a sequence of planar two-dimensional grids with decreasing coarseness. See figure 3(*b*).

(*c*) Analysis of local deformation pattern, determining the eigenvalues and eigenvectors of $\boldsymbol{F}$, determining if there is an unit eigenvalue. If so, then the eigenvector that corresponds to unit eigenvalue is determined (this vector is tangential to the periodic line) and used to step along the periodic line (see figure 1).

(*d*) Back to step (*b*) to proceed along the periodic line.

(*e*) Diagnose the type of periodic points. See § 2.2.

The strategy starts with a relatively coarse uniform three-dimensional rectangular grid of material points in the flow domain. For computational reasons, the grids are such that they do not touch the boundaries. The points of these grids are tracked over one complete period of motion and the total displacement of each individual point $d(\boldsymbol{X})$ is computed. The minima of this function indicate the location of (possible) periodic points.

(*a*)

(*b*)
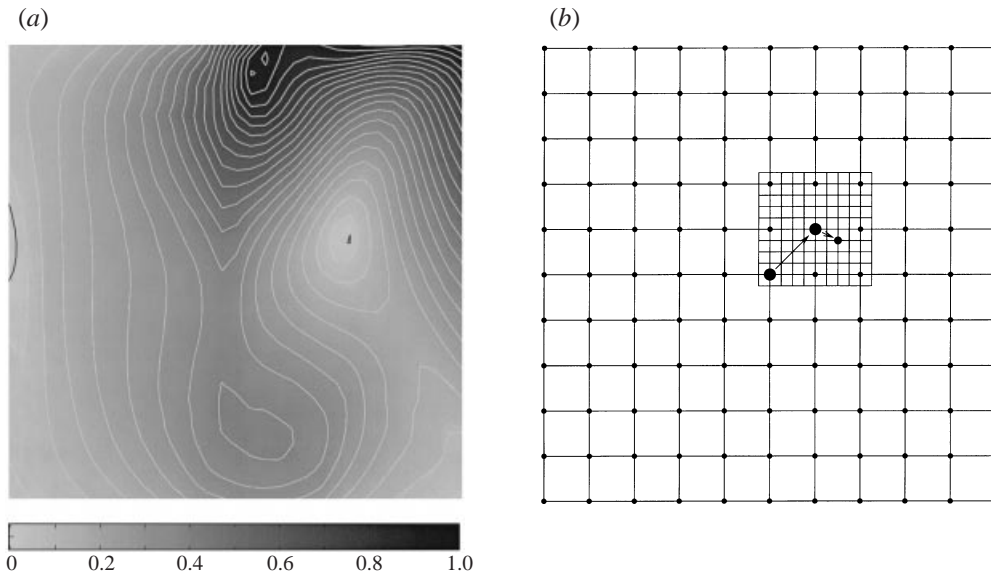
FIGURE 3. (*a*) Greyscale plot representing the displacement $d(X)$ of a marker grid over one period; (*b*) refined marker grid, used to locate the local minimum of displacement.

As the resolution of the grid is limited (by computational resources), there is no confidence that the local minima indeed represent the periodic structures. Therefore, these regions of low displacement are refined by recomputing $d(X)$ on a finer grid (see figure 3) and again analysed until a minimum is found that is, within some specific tolerance, close enough to zero.

In addition to the displacement analysis of the points in the uniform three-dimensional rectangular grid, extra points are added around the original set of points. The differences in displacement of the new set of points after one complete period of motion are used to determine the stretching $s(X)$ in the original material points. Finally, the eigenvector that corresponds to the unit eigenvalue is determined and a search direction is determined to capture the *route* of the periodic line, see also figure 1. It should be noted that if the initial grid is not fine enough, periodic points may stay unnoticed. For the three-dimensional cavity flows analysed in this paper a $32 \times 32 \times 32$ grid was found fine enough to locate an initial guess for the position for the periodic points.

4. Results and discussion

First, the accuracy of the numerically obtained velocity field and the particle tracking algorithm is addressed. The results for the general method for finding periodic structures are compared with results using symmetry of the flow. The application of our method for the determination of periodic structures in general three-dimensional time-periodic flows is addressed in the last section. Here, a four-step mixing protocol is introduced and the periodic structures found in this flow are analysed.

4.1. *Accuracy of the velocity field and the particle tracking algorithm*

To check the accuracy of the numerical techniques used to locate periodic points, a well-known two-dimensional example of a periodic mixing flow in a rectangular

(*a*)   (*b*)
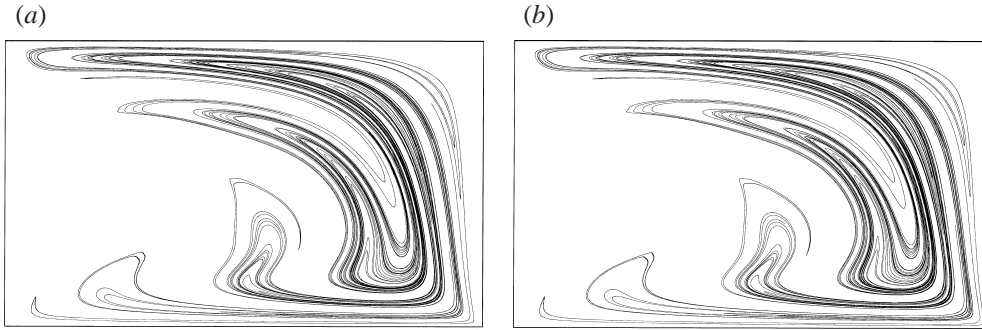
FIGURE 4. The results of tracking a blob after five periods using a numerical (*a*) and an analytical (*b*) velocity field. The dimensionless displacement *DD* is equal to 6.24.

cavity is considered (later this flow is extended to the three-dimensional case). The flow is generated by successive periodic motion of two opposite walls (upper and lower in figure 4) in opposite directions. The two other walls are fixed. First, during the first half-period the top wall moves to the right, then, during the second half-period the bottom wall moves to the left. This mixing flow is chosen since for this flow a semi-analytical solution is available (Meleshko & Peters 1996) so the accuracy of the numerical scheme in computing the velocity velocity field can be validated. The dimensionless displacement of each wall during a period is defined as

$$D = \frac{d_{top} + d_{bot}}{w}, \tag{4.1}$$

where d_{top} and d_{bot} are the displacement of the top and bottom, respectively, while w denotes the width of the cavity. For this case the dimensionless displacement was set equal to $D = 6.24$, the same value as used by Ottino (1989) where $d_{top} = d_{bot}$. The aspect ratio of the cavity (length to width) was 5:3. A blob is placed around a first-order hyperbolic point (1.15, 0) and is tracked for five periods using both the numerical and the analytical solution. The numerical solution is obtained using a spectral element mesh consisting of 32 elements of 8th order. The results, presented in figure 4, show a nearly perfect agreement between both deformed blobs, justifying the use of the numerical solution technique.

The number of material points needed to describe the blob is presented in table 1. The table shows the exponential increase of the circumference of the blob (between each period approximately a factor $3\frac{1}{2}$). The number of points needed to describe the blob increases approximately the same factor. During by tracking over five periods the area is computed for the numerical and analytical situations. In both cases the area preservation is exceptionally good, demonstrating the accuracy of the adaptive particle tracking scheme used.

4.2. *Protocol definition of three-dimensional periodic flows*

Three different prototype mixing flows with increasing complexity have been analysed for first-order periodic points. Figure 5 displays the protocols of wall motion used to generate the mixing flows. The flow field is described by the Stokes equations (3.2) and the boundary conditions (3.1).

The specific boundary conditions used are as follows (*n* is a positive integer denoting
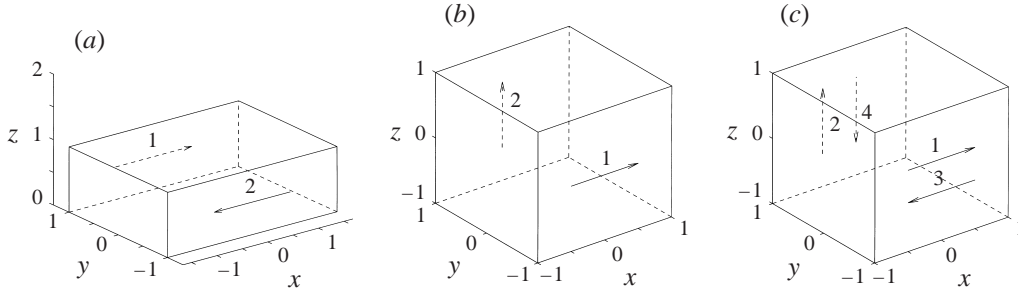
FIGURE 5. Protocols $\mathscr{A}, \mathscr{B}$ and $\mathscr{C}$ (*a–c*). The sequence and the direction of the front and back wall motion is shown. All other walls are fixed.

Time in periods T	0	1	2	3	4	5
Number of points (analytical)	120	207	627	2728	9217	30739
Circumference of blob	1	10.0650	31.9198	136.7518	442.1563	1489.7207
Area of blob	1	1.0042	0.9985	0.9957	1.0071	1.0041
Number of points (numerical)	120	205	624	2687	9139	30367
Circumference of blob	1	9.9461	31.6231	135.2885	438.6018	1473.1791
Area of blob	1	1.0041	0.9986	0.9902	1.0018	0.9830

TABLE 1. Comparison of the number of points, area and circumference between the numerical and analytical results as presented in figure 4. The values for area and circumference are relative to the initial configuration.

the period number and T is the total period time):

$$\text{Protocol } \mathscr{A}$$
$$U_F = 1, \quad nT < t \leqslant (n + \tfrac{1}{2})T;$$
$$U_B = 1, \quad (n + \tfrac{1}{2})T < t \leqslant (n+1)T;$$
$$\text{Protocol } \mathscr{B}$$
$$U_F = 1, \quad nT < t \leqslant (n + \tfrac{1}{2})T;$$
$$W_B = 1, \quad (n + \tfrac{1}{2})T < t \leqslant (n+1)T;$$
$$\text{Protocol } \mathscr{C}$$
$$U_F = 1, \quad nT < t \leqslant (n + \tfrac{1}{4})T;$$
$$W_B = 1, \quad (n + \tfrac{1}{4})T < t \leqslant (n + \tfrac{1}{2})T;$$
$$U_F = -1, \quad (n + \tfrac{1}{2})T < t \leqslant (n + \tfrac{3}{4})T;$$
$$W_B = -1, \quad (n + \tfrac{3}{4})T < t \leqslant (n+1)T.$$

Mixing protocol $\mathscr{A}$ is a straightforward extension of the two-dimensional protocol. Protocols $\mathscr{B}$ and $\mathscr{C}$ have been introduced to increase the three-dimensional effects in the mixing flows. For protocol $\mathscr{A}$ the dimensionless displacement D of the walls over a half-period was equal to 7. For protocol $\mathscr{B}$ the range $3 \leqslant D \leqslant 5$ was considered
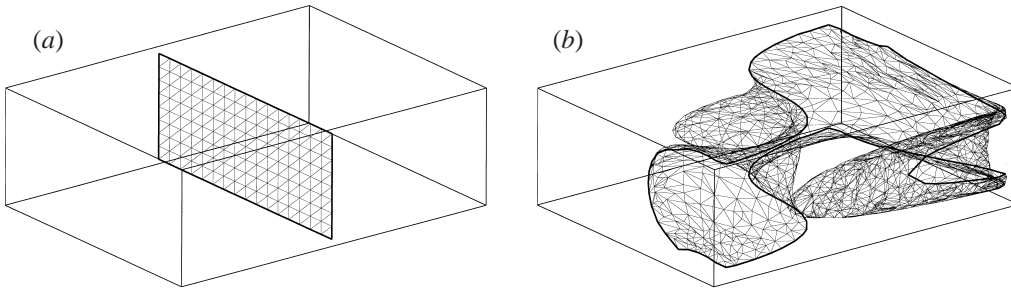
FIGURE 6. (*a*) The initial planar surface which is tracked using mixing protocol $\mathscr{A}$ from a quarter to three quarters of a period (*b*). For the initial surface a uniform grid is chosen which is adaptively refined during the tracking procedure.

and for protocol $\mathscr{C}$ the cases $D = 3$ and $D = 5$ are examined. The box size for protocol $\mathscr{A}$ was chosen such that results can be compared with two-dimensional results ($h = 1, w = 1.67, d = 1$). For the other protocols a cube, $-1 < x < 1$, $-1 < y < 1$, $-1 < z < 1$, is chosen so that only one velocity field is required.

4.3. *Analysis of periodic structures in mixing flow $\mathscr{A}$*

The periodic lines for the rectangular cavity found by using symmetry conditions serve as an useful example to check the general technique introduced in §2.2. Figure 6 shows the deformation of the initial planar surface, which is tracked from a quarter to three quarters of a period. The intersection of the two surfaces (which are lines for this flow with dimensionless displacement equal to 7) is tracked to a full period and provides the location of periodic points. The periodic structures, which are now lines instead of points, are presented in figure 7. The thickness of the line is used to designate its type: stable (elliptic) lines are plotted thick, unstable (hyperbolic) are plotted thin. The symmetry, which is present for this flow, is also revealed by the periodic points. The planes of symmetry are the mid-plane $z = 0.5$ and the plane $y = 0$. Note that the periodic lines displayed in figure 7 do not end at the boundaries of the flow domain. This is merely because of computational reasons: the initial surface is not touching the boundaries.

The pattern shown in figure 7 can be related to the results for the two-dimensional cavity flow with decreasing D, noticing that in the vicinity of the lid and bottom, the effect of the wall displacement is reduced, and that the motion of the particles is, approximately, restricted to one horizontal level. Close to the bottom only one periodic line is formed, similar to one periodic point in two dimensions, for relatively small values of D. Approaching the mid-plane, equivalent to increasing effective D, the single elliptic line is split into two elliptic lines and one hyperbolic line. Closer to the mid-plane ($z = 0.5$) the elliptic lines also change their type and become hyperbolic. Another typical phenomenon, already known from the two-dimensional case, is the birth of a pair of periodic points of different type 'out of nothing'. This is observed in the left half of the cavity ($x < 0$) where a closed ring is formed when the opposite lid is approached and the lines merge and disappear again.

Analysis of periodic structures in flow $\mathscr{A}$ using a general technique

Mixing flow $\mathscr{A}$ is also analysed using the *general* technique introduced in §2.2. The easiest way to examine the three-dimensional structures is 'slice by slice' (step (*b*) in the algorithm). In figure 8 the patterns of the displacement and the stretching ratio are presented for a number of horizontal cross-sections. On the left side the total
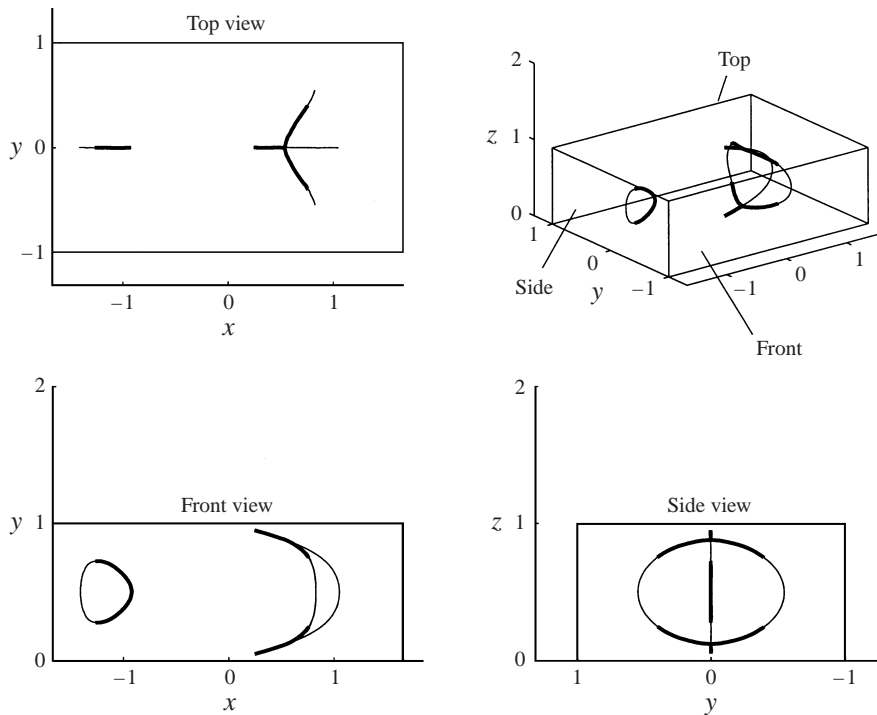
FIGURE 7. Periodic lines in the quasi-two-dimensional flow (mixing protocol $\mathscr{A}$) : thin – unstable (hyperbolic) lines; thick – stable (elliptic) lines, derived using the symmetry of the flow field.

displacement $d(X)$ over one period is presented. Light coloured regions represent regions of low displacements, whereas the dark coloured regions are regions of high displacements. On the right side of the figure, the stretching $s(X)$ over one period is depicted. To increase the clarity of the map, thresholding of the maximum stretching values was used (the threshold level was equal to 5). To determine the type of the periodic points, contour lines for displacement are placed on the stretching figures.

Close to the bottom, at the level $z = 0.05$ (see figure 8), the local minimum of the displacement in the zone of low stretching indicates that the elliptic line crosses this plane. The horizontal slice $z = 0.125$ is, approximately, the level where a periodic line is split into three (compare with figure 7). This phenomenon is indicated by the shape of the zone of the local minimum of displacement. The 'tongue' of the high-stretching region (green colour in figure 8), approaching the central zone of the displacement minimum, indicates that, after the splitting, the line in the middle becomes hyperbolic. On the upper level, $z = 0.225$, three separate lines, crossing the plane, are clearly visible: one of them in the middle, located at the $y = 0$ axis being of the hyperbolic type, while the two other lines remain of the elliptic type. In the mid-plane, $z = 0.5$, all three sharp local minima of displacement are positioned in zones of high stretching ratio, indicating that the points are of hyperbolic type. In the left part of the cross-section, a clear portrait of another elliptic periodic line is present. This line is part of the closed curve in the left of the cavity, plotted in figure 7. The coupled hyperbolic part of the line is outside the zone in which the analysis was performed. It can be concluded that the results of this 'displacement-stretching' analysis are in excellent agreement with the results of the search for periodic structures using the 'symmetry' algorithm.

(*a*)   Displacement $d(X)$ (*b*)   Stretching $s(X)$

$z = 0.050$

$z = 0.125$

$z = 0.225$

$z = 0.500$
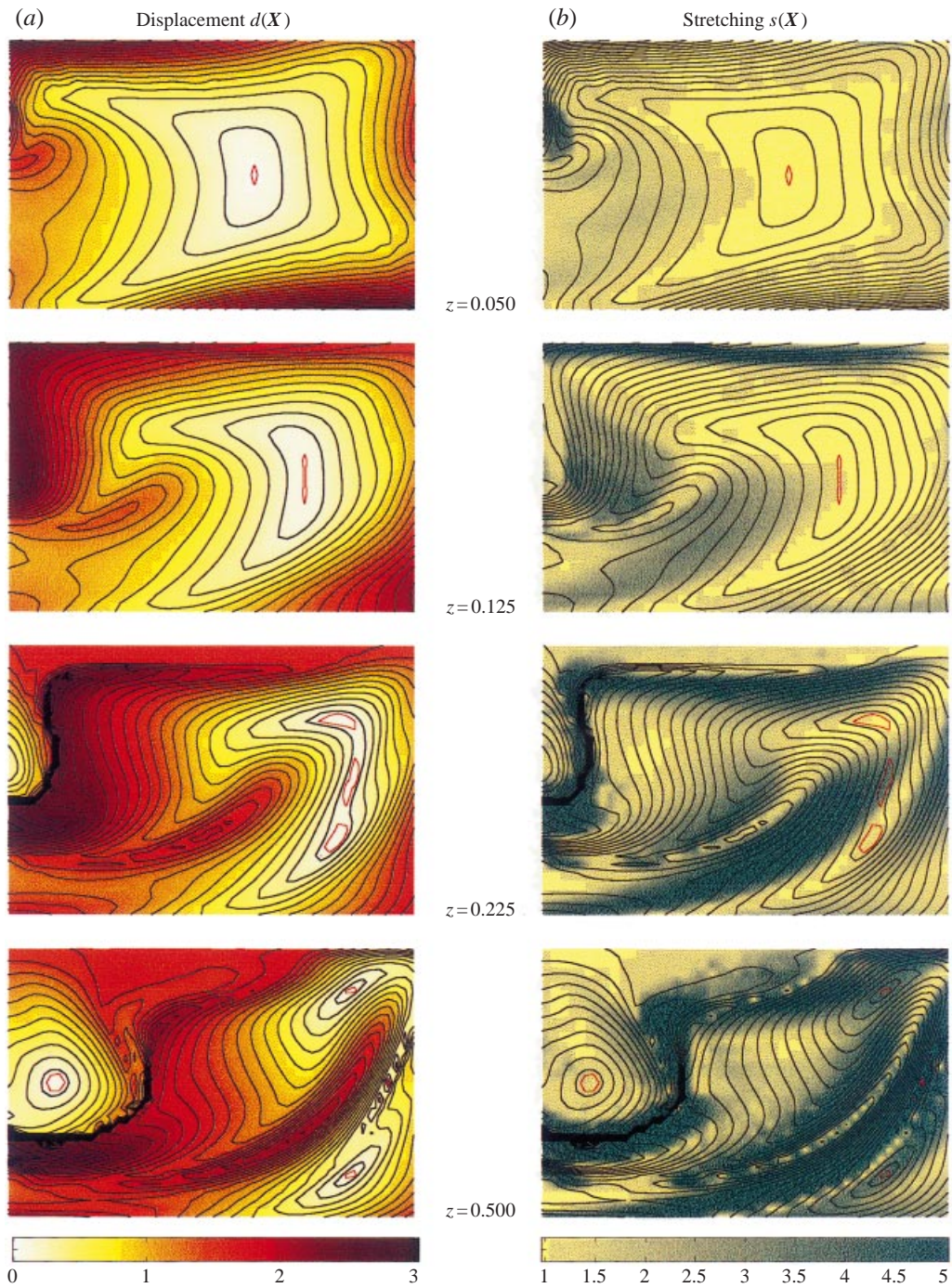
FIGURE 8. Maps of displacement and stretching over one period of motion (using mixing protocol $\mathscr{A}$) at the horizontal levels $z = 0.05, 0.125, 0.225$ and 0.5, respectively, with ranges $[-0.9w < x < 0.9w, -0.9d < y < 0.9d]$. (*a*) Maps of displacement: colours denote displacement; white colour corresponds to low displacement. Red contour line denotes the area of minimum displacement. (*b*) Maps of the stretching: colours denote the stretching ratio, green corresponds to high stretching, yellow the low stretching.

Point	$\Delta x = 10^{-1}$	$\Delta x = 5 \times 10^{-2}$	$\Delta x = 2.5 \times 10^{-2}$	$\Delta x = 1.25 \times 10^{-2}$	$\Delta x = 6.25 \times 10^{-3}$
$\boldsymbol{p}_1$	0.99567	0.99846	0.9995	0.9997	0.9998
$\boldsymbol{p}_2$	0.99873	0.99569	1.0004	1.0002	1.0000
$\boldsymbol{p}_3$	1.00291	1.00037	1.0001	1.0000	1.0000

TABLE 2. The computed unit eigenvalues of the displacement gradient matrix for the points $\boldsymbol{p}_1, \boldsymbol{p}_2$ and $\boldsymbol{p}_3$; The point $\boldsymbol{p}_2$ is an elliptic periodic point, the other two are of hyperbolic type. The eigenvalues are computed using a second-order central differences scheme with spatial discretisation step size Δx.

Table 2 contains the unit eigenvalues determined for the points $\boldsymbol{p}_1 = (0.829, -0.548, 0.509)$, $\boldsymbol{p}_2 = (0.717, -0.336, 0.207)$ and $\boldsymbol{p}_3 = (1.051, -1.657, 0.510)$. The point $\boldsymbol{p}_2$ is an elliptic periodic point, the other two are of hyperbolic type. The results show that the eigenvalues are accurately computed. The periodic points are therefore located on a periodic line.

4.4. *Analysis of periodic structures in mixing flow $\mathscr{B}$*

The protocol of mixing flow $\mathscr{B}$ is another extension of the two-dimensional cavity flow to a three-dimensional cavity flow by moving one wall perpendicular to the other. For this protocol no first-order periodic points, and therefore also no related periodic structures, were found. Higher-order periodic points were not investigated.

Figure 9 shows, for a number of slices of the flow domain, the displacement of the initial grid after one period and with $D = 3$. The minimum displacement is always significantly larger than the grid cell size which is used to evaluate the displacement. This analysis was done for a range of values for the displacement parameter $D = 3$–5, but no (first-order) periodic points were detected. The absence of first-order periodic points for this mixing protocol can also be explained by using a more qualitative argument. If a periodic point exists, then the closed trajectory of this point consists of two parts, each stemming from the streamlines of the two half-periods (see figure 10). These streamlines are nearly planar during each half-period ($z = $ const for the first half-period and $x = $ const for the second one), and their pattern looks the same as for a two-dimensional cavity. It is typical for such a pattern that streamlines are closer to the driving wall than to opposite wall. This means that crossing streamlines from the two half-periods, belonging to streamline patterns created by opposite driving walls, cannot cross in any other part of the flow domain, and therefore they cannot form the closed trajectory which is needed for periodic points.

Detecting the absence of first-order periodic points in a mixing flow is an important result as it gives an early, strong indication of poor mixing properties.

4.5. *Analysis of periodic structures in mixing flow $\mathscr{C}$*

For this four-step protocol, the flow was induced by the successive motion of the two opposite walls in opposite directions as depicted in figure 5. The net resulting displacement of each wall, after one complete period, is zero. Different from the previous protocols is that now slices in three directions were used for the analysis, because the configuration of the lines was completely unknown, and there was no information about their possible position. Again, first coarse grids were used to locate an initial guess for the position of the periodic points. A sequence of finer, locally refined grids provided a more accurate location. For these points, where $d(X) < \epsilon$, the eigenvalues and eigenvectors of $\boldsymbol{F}_X$ are determined. The eigenvector that corresponds
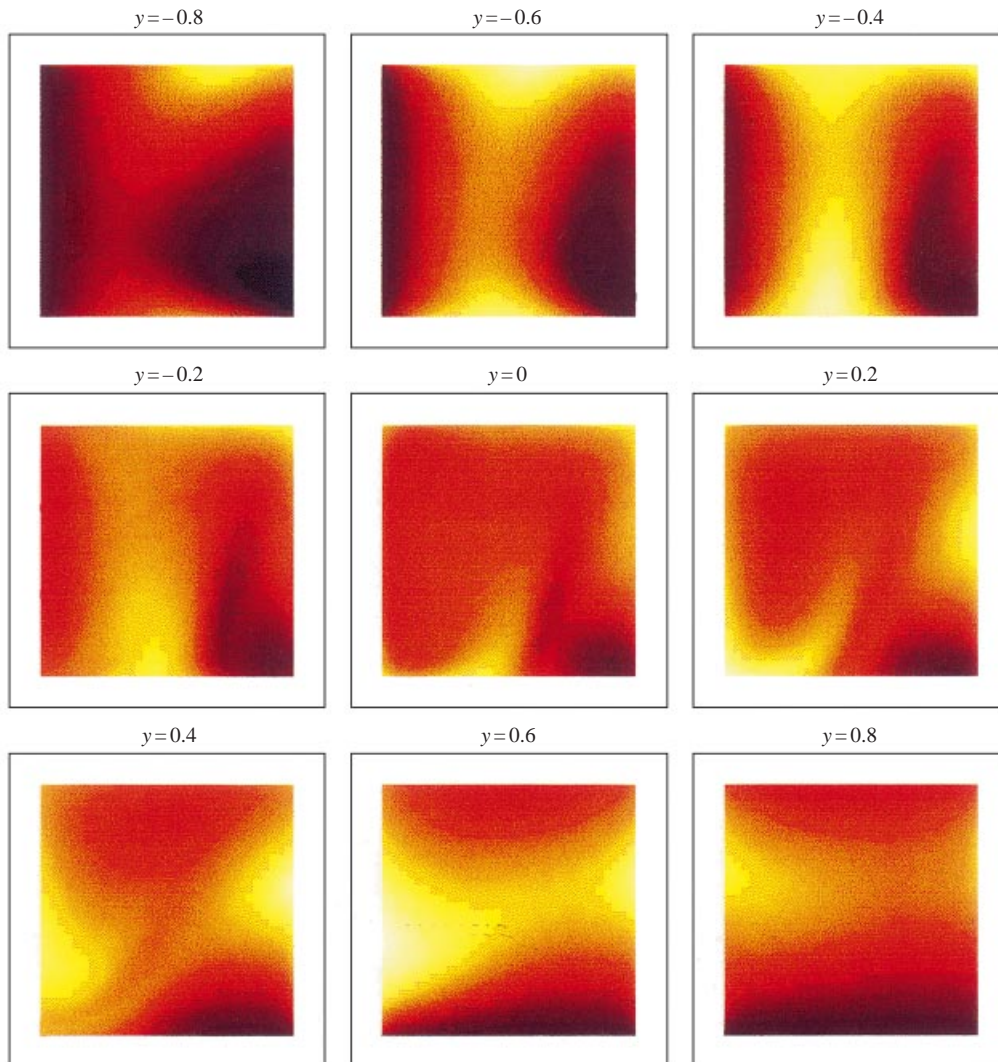
FIGURE 9. Maps of displacement over one period of the two-step motion ($D = 3$) using mixing protocol $\mathscr{B}$ at the levels $y = -0.8, -0.6, \cdots, 0.8$ respectively with ranges $[-0.9 < x < 0.9,\ -0.9 < y < 0.9]$. Colours denote displacement; lighter colours correspond to low displacement.

to the unit eigenvalue is determined and a search direction is determined to capture the periodic line (figure 1). As a result, a system of periodic lines was revealed for $D = 3$ and $D = 5$.

The periodic lines found are plotted in figures 11(a) and 11(b). Hyperbolic parts of the lines are plotted thin, elliptic lines are displayed thick. For both D-values three periodic lines are formed. In the first case, $D = 3$, two completely elliptic lines are revealed and one periodic line consisting of one elliptic part and two hyperbolic tips. In the case $D = 5$ the periodic structure consists of three lines with mixed types of periodic points. The existence of first-order hyperbolic points for both D-values shows that mixing protocol $\mathscr{C}$ can lead to chaotic advection.

To emphasize the importance of the periodic structure analysis, the motion of two blobs is calculated for a small number of periods. One blob is positioned around
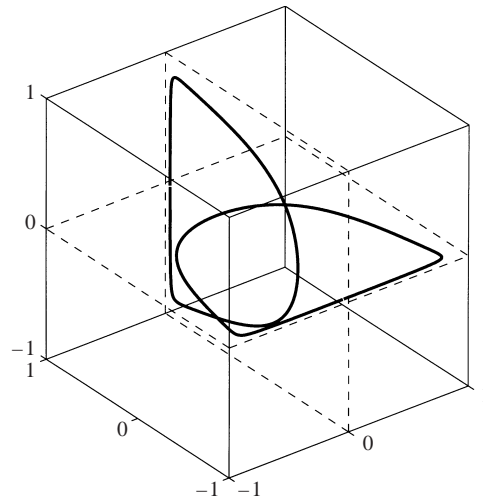
FIGURE 10. Two streamlines of mixing flow $\mathscr{B}$, one belonging to the movement of the front wall and the other to the back wall: it is clear that it is not possible for a particle to travel over streamlines and return to its original position.
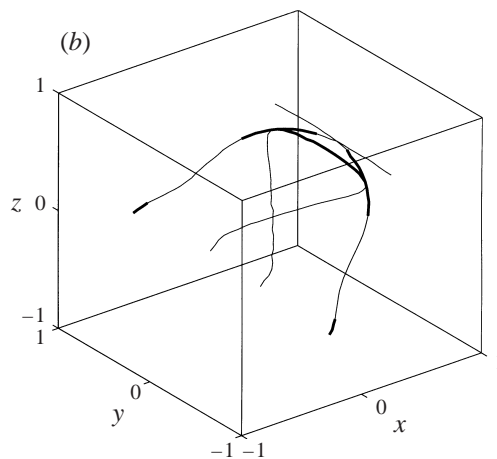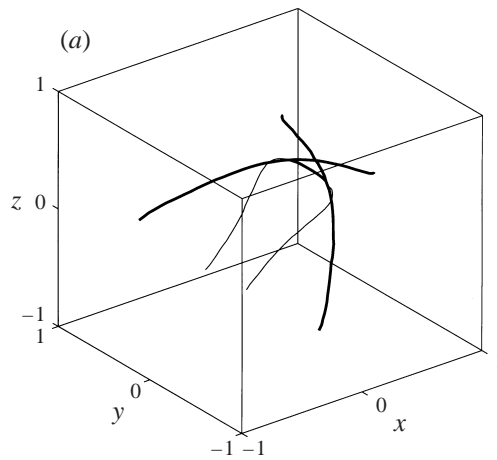
FIGURE 11. Periodic lines in the four-step mixing flow (protocol $\mathscr{C}$) : thin – unstable (hyperbolic) lines; thick – stable (elliptic) lines. (*a*) $D = 3$, (*b*) $D = 5$.
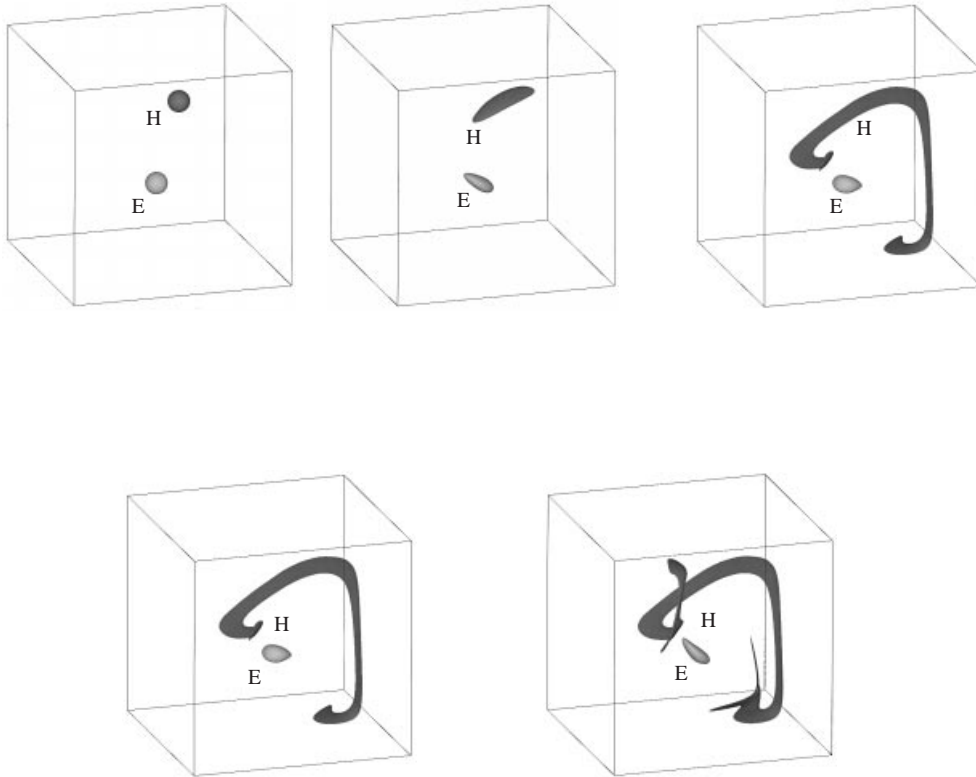
FIGURE 12. Deformation of two blobs after four periods: initial blob-around a hyperbolic point, and blob E around an elliptic point.
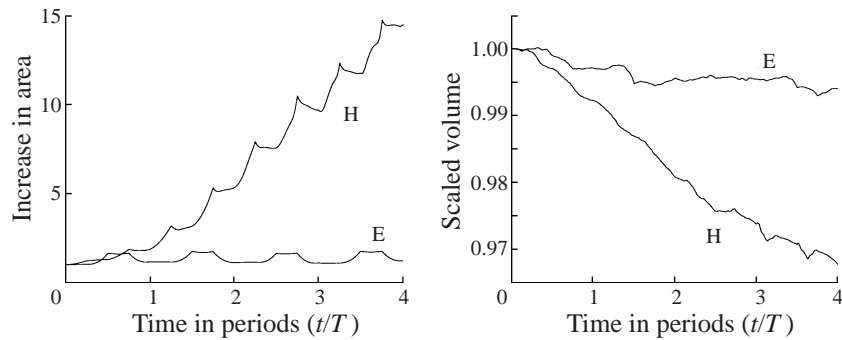
FIGURE 13. Increase in interfacial area and volume conservation of elliptic (E) and hyperbolic (H) blob for four-step cavity flow (mixing protocol $\mathscr{C}$).

an elliptic point, the other one around a hyperbolic point. The results for the case $DD = 3$ are presented in figure 12. The difference in deformation of the blobs is large and the blob around the hyperbolic point is advected through the whole domain, while the stretching of the blob around the elliptic point is only minor. In figure 13 results regarding the volume conservation are depicted. For the material blobs around the hyperbolic and elliptic points, it is shown that the volume is preserved within a few percent after four periods of mixing. The area is scaled with respect to the area of the initial blob. For the blob around the elliptic part of the line, the area remains

nearly constant; however for the hyperbolic blob a substantial increase in area is observed. As a final test a material point (0.188562, −0.399432, −0.408048) located at an elliptic line is tracked for 500 periods. The distance between the tracked and original points is 0.0062 indicating the accurate location of the elliptic point.

5. Conclusions

A method is presented to determine periodic structures in three-dimensional mixing cavity flows. This method is also applicable to more general flows and geometries. The analysis of the motion during one period provides information on deformation and stretching in the flow. Careful investigation of these data results in the location of periodic points (if any) in the flow domain. Analysis of the displacement gradient matrix is used to identify the type of the periodic points. A major result is that *periodic lines* are observed for these three-dimensional cavity flows. The structure of the lines can be rather complex in geometry and their nature can change along the line from elliptic to hyperbolic.

The results show that the approach to locate and identify periodic structures has successfully been applied to several three-dimensional cavity flows. Two different two-step mixing protocols, as well as a four-step protocol in cavity flows were analysed. The periodic structures in the first two-step mixing flow, with parallel moving walls, are found using two techniques: one exploits symmetry in the flow and is used to validate the other technique using a more general approach. Convergence of the latter has been demonstrated numerically by evaluation of the eigenvalues of the displacement gradient matrix. Both methods lead to the same set of periodic structures. For the second two-step mixing protocol, where one wall moves in a direction perpendicular to the other wall, no first-order periodic points were found. Thus, the method developed not only locates periodic points, but also provides the important information that periodic structures are absent, i.e. the mixing protocol used appears to be less appropriate compared to other protocols with first-order hyperbolic periodic points. For the third four-step protocol periodic structures were found for two different mixing parameters. The tracking of two blobs located around periodic points of hyperbolic and elliptic type, respectively, shows the large difference in stretching in the four-step induced periodic flow. Also, the high accuracy of the method is revealed by the (nearly) constant location of the blob around an elliptic point.

REFERENCES

AREF, H. 1984 Stirring by chaotic advection. *J. Fluid Mech.* **143**, 1–21.

AVALOSSE, T. & CROCHET, M. J. 1997 Finite element simulation of mixing: 2. Three-dimensional flow through a Kenics mixer. *AIChE J.* **43**, 588–597.

BAJER, K. 1995 Hamiltonian formulation of the equations of streamlines in three-dimensional steady flows. In *Choas Applied to Fluid Mixing*. Elsevier.

CAREY, G. F. & CHEN, Y. 1995 Simulation of fluid mixing using least-squares finite elements and particle tracing. *Intl J. Numer. Heat Fluid Flow* **5**, 549–573.

CARTWRIGHT, J. H., FEINGOLD, M. & PIRO, O. 1996 Chaotic advection in three-dimensional unsteady incompressible flow. *J. Fluid Mech.* **316**, 259–284.

CHIEN, W. L., RISING, H. & OTTINO, J. M. 1986 Laminar mixing and chaotic mixing in several cavity flows. *J. Fluid Mech.* **170**, 355–377.

GRESHO, P. M. 1990 On the theory of semi-implicit projection methods for viscous incompressible flow and its implementation via a finite element method that also introduces a nearly consistent mass matrix. part 1: Theory. *Intl J. Numer. Meth. Fluids* **11**, 587–620.

HOBBS, D. M. & MUZZIO, F. J. 1997 Effects of injection location, flow ratio and geometry on Kenics mixer performance. *AIChE J.* **43**, 3121–3132.

JANA, S. C., METCALFE, G. & OTTINO, J. M. 1994 Experimental and computational studies of mixing in complex Stokes flows: The vortex mixing flow and multicellular cavity flows. *J. Fluid Mech.* **269**, 199–246.

KUSCH, H. A. & OTTINO, J. M. 1992 Experiments on mixing in continuous chaotic flows. *J. Fluid Mech.* **236**, 319–348.

MADAY, Y. & PATERA, A. T. 1989 Spectral element methods for the incompressible Navier–Stokes equations. In *State-of-the-Art Surveys on Computational Mechanics* (ed. A. Noor). ASME, New York.

MELESHKO, V. V. & PETERS, G. W. M. 1996 Periodic points for two-dimensional Stokes flow in a rectangular cavity. *Phys. Lett.* A **216**, 87–96.

MILES, K. C., NAGARAJAN, B. & ZUMBRUNNEN, D. A. 1995 Three-dimensional mixing of fluids in a cylindrical cavity. *Trans. ASME: J. Fluids Engng* **117**, 582.

MINEV, P. D., VOSSE, F. N VAN DE, TIMMERMANS, L. J. P. & STEENHOVEN, A. A. VAN 1995 A second order splitting algorithm for thermally-driven flow problems. *Intl J. Numer. Heat Fluid Flow* **6**, 51–60.

OTTINO, J. M. 1989 *The Kinematics of Mixing: Stretching, Chaos and Transport.* Cambridge University Press.

OTTINO, J. M. 1990 Mixing, chaotic advection and turbulence. *Ann. Rev. Fluid Mech* **22**, 207–253.

PATERA, A. T. 1984 A spectral element method for fluid dymanics: laminar flow in a channel expansion. *J. Comput. Phys.* **54**, 468–488.

PRESS, W. H., TEUKOLSKY, S. A., VETTERLING, W. T. & FLANNERLY, B. P. 1992 *Numerical Recipes in Fortran*, 2nd Edn. Cambridge University Press.

SOUTHERLAND, K., FREDERIKSEN, R. & DAHM, W. 1995 Comparison of mixing in chaotic and turbulent flows. In *Chaos Applied to Fluid Mixing*. Elsevier.

SOUVALIOTIS, A., JANA, S. C. & OTTINO, J. M. 1995 Potentialities and limitations of mixing simulations. *AIChE J.* **41**, 1605–1621.

TIMMERMANS, L. J. P., MINEV, P. D. & VOSSE, F. N. VAN DE 1996 An approximate projection scheme for incompressible flow using spectral elements. *Intl J. Numer. Meth. Fluids* **22**, 673–688.